

## Anomalous sound velocities in polycrystalline MgO under non-hydrostatic compression

A. E. Gleason,<sup>1</sup> H. Marquardt,<sup>2</sup> B. Chen,<sup>1</sup> S. Speziale,<sup>2</sup> J. Wu,<sup>3</sup> and R. Jeanloz<sup>1</sup>

Received 14 October 2010; revised 21 December 2010; accepted 3 January 2011; published 5 February 2011.

[1] Brillouin scattering from polycrystalline MgO (periclase) non-hydrostatically compressed to, and decompressed from, 60 GPa at room temperature documents shear- and compressional-wave velocities  $\sim 20\%$  lower than values measured under hydrostatic compression. Calculations reveal that wave velocities can be lowered due to the elastic effects of non-hydrostatic stresses, but by only a few percent. Neither these elastic effects nor preferred orientation can account for the reduction in the sound velocity.

**Citation:** Gleason, A. E., H. Marquardt, B. Chen, S. Speziale, J. Wu, and R. Jeanloz (2011), Anomalous sound velocities in polycrystalline MgO under non-hydrostatic compression, *Geophys. Res. Lett.*, 38, L03304, doi:10.1029/2010GL045860.

### 1. Introduction

[2] Elastic properties of minerals reveal Earth's internal structure through the interpretation of seismic models based on compressional- and shear-waves and normal modes [e.g., *Ishii and Tromp*, 1999]. The internal dynamics of Earth, however, involve non-hydrostatic stresses that drive plate tectonics, trigger earthquakes, deform the lithosphere and define the long-term evolution of our planet's interior [e.g., *Watts*, 1978; *Kanamori*, 1980; *Chung and Kanamori*, 1980; *Munguia and Brune*, 1984; *Fukao and Kikuchi*, 1987; *Kanamori et al.*, 1998; *Ruff*, 1999; *Conrad and Hager*, 1999; *Buffett*, 2006; *Kaus et al.*, 2009].

[3] In order to understand the effects of non-hydrostatic stresses on elastic wave velocities of minerals in Earth's mantle we make acoustic wave-velocity measurements on polycrystalline samples because single crystals cannot sustain large non-hydrostatic stresses. We use Brillouin spectroscopy, which has been shown to yield reliable values for seismic wave velocities from both single crystals and polycrystals taken to large (quasi-) hydrostatic pressures [e.g., *Campbell and Heinz*, 1992; *Marquardt et al.*, 2009; *Murakami et al.*, 2009; *Gleason et al.*, 2009; *Chen et al.*, 2010]. Our focus here is on MgO (periclase), because it is the end member composition of ferropericlase (Mg,Fe)O that is a major component of Earth's deep mantle. Periclase also serves as an important standard in mineral physics [e.g., *Jackson and Niesler*, 1982].

[4] MgO is stable in the NaCl-type (*B1*) crystal structure (*Fm $\bar{3}m$* ) to the bottom of the mantle; being cubic, it has 3 independent second-order elastic moduli ( $c_{11}$ ,  $c_{12}$  and  $c_{44}$ ). We use three initial sample types: 1) MgO powder ground to 5–10  $\mu\text{m}$  particle size, verified via optical microscopy (particles may not be single crystals, Mallinckrodt, Analytical reagent #6015, 99.3% purity); 2) 1  $\mu\text{m}$  particle size powder MgO, verified via BET analysis (American Elements, MG-OX-03-P, 99.9% purity); and 3) 6  $\mu\text{m}$  average grain size sintered translucent MgO [*Chen et al.*, 2008].

[5] Brillouin spectra were collected in two scattering geometries – equal-angle transmission, and backscatter – using 0.50 W of polarized 532 nm radiation from a continuous-wave Nd:YVO<sub>4</sub> laser, along with confocal optics and a Sandercock six-pass tandem Fabry-Perot interferometer [*Gleason et al.*, 2009]. For equal-angle transmission (external scattering angle  $\theta$ ) with a parallel-sided platelet sample,  $\Delta\omega$  is the measured frequency shift,  $\lambda_0$  is the incident laser wavelength, and the wave velocities for shear ( $V_s$ ) or compressional ( $V_p$ ) modes are given by  $V_{s,p} = (\Delta\omega)\lambda_0/2 \sin(\theta/2)$ . All experiments use a short, symmetric diamond-anvil cell, with 300  $\mu\text{m}$  culet diamonds and a 130  $\mu\text{m}$  hole in a stainless steel gasket (pre-indented to a final thickness of 50  $\mu\text{m}$ ) serving as the pressure chamber. Pressure is calibrated by ruby fluorescence [*Mao et al.*, 1978].

[6] To check the reliability of our method, we first study polycrystalline MgO under quasi-hydrostatic loading. The 6  $\mu\text{m}$  sintered MgO was polished to 30  $\mu\text{m}$ , sliced to a  $75 \times 75 \mu\text{m}$  square and loaded in a 50  $\mu\text{m}$  thick gasket along with  $< 1\text{--}2 \mu\text{m}$  diameter ruby spheres (as calibrant) and 4:1 methanol:ethanol (ME) mixture as pressure-transmitting medium. We see no evidence of ME peaks in any of the Brillouin spectra, including at pressures where the ME compressional mode would stand alone [*Armstrong et al.*, 2008]. Ruby spheres also did not give a Brillouin signal. Due to intense grain-boundary (elastic) scattering, we were unable to collect useful Brillouin signals from loose powder samples under hydrostatic loading.

[7] For non-hydrostatic loading, powder is placed on bare culets and pressed together to form a semi-transparent disc of  $\sim 50 \mu\text{m}$  thickness on one culet face. After decompression, radial cracks form in the MgO [e.g., *Meade and Jeanloz*, 1988, Figure 6b]. On the opposite culet 5–8 ruby spheres, each  $< 1\text{--}2 \mu\text{m}$  in diameter, are distributed across the chamber to monitor pressure. The hole in the gasket slices through the polycrystalline MgO disc in a cookie-cutter fashion when the cell is closed, thus creating the sample used for the measurements. A similar procedure is followed for non-hydrostatically loading the 6  $\mu\text{m}$  sintered MgO, with the original sintered polycrystalline wafer

<sup>1</sup>Department of Earth and Planetary Science, University of California, Berkeley, California, USA.

<sup>2</sup>GFZ German Research Centre for Geosciences, Potsdam, Germany.

<sup>3</sup>Material Sciences Division, Lawrence Berkeley National Laboratory, Berkeley, California, USA.

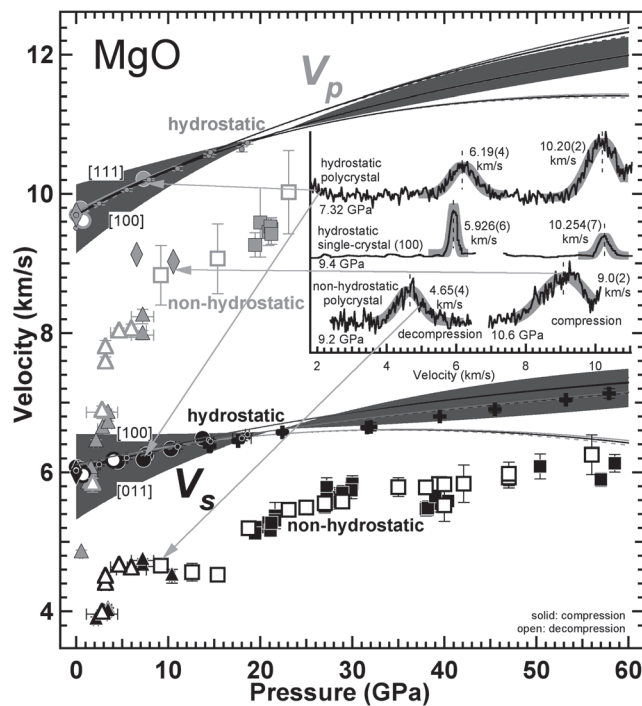


**Figure 1.** Pressure dependence of the compressional and shear acoustic velocity of polycrystalline MgO. Grey symbols: compressional mode; black symbols: shear mode. Large and small circles are hydrostatically loaded, sintered MgO wafers in methanol:ethanol and calculated single-crystal averages [Sinogeikin and Bass, 2000; Spetzler, 1970], respectively; black crosses: Murakami *et al.* [2009]. Voigt (solid upper), Reuss (dashed lower) and Hashin-Shtrikman (solid black inner) bounds are provided for each single crystal dataset [Bateman *et al.*, 1961; Simmons and Wang, 1971; Schreiber *et al.*, 1973; Birch, 1978]; Bogardus [1965] (upper-most trio of curves for  $V_p$  and  $V_s$ ), Sinogeikin and Bass [2000] (middle), and Jackson and Niesler [1982] (lower-most). Dark grey shaded area indicates the range of single crystal absolute maximum and minimum  $V_s$  and  $V_p$  [Sinogeikin and Bass, 2000; Schreiber *et al.*, 1973]. Non-hydrostatically loaded polycrystals: squares (5–10  $\mu\text{m}$  pressed powder); triangles (1  $\mu\text{m}$  pressed powder); diamonds (6  $\mu\text{m}$  sintered). *Inset:* spectra of hydrostatically and non-hydrostatically loaded samples at 7–10 GPa, compression and decompression for our polycrystalline sample, and for a hydrostatically loaded single crystal of  $(\text{Mg}_{0.987}\text{Fe}_{0.013})\text{O}$  [100] [Reichmann *et al.*, 2008].

(450  $\mu\text{m}$  thick) polished on both sides down to 50  $\mu\text{m}$  thickness.

[8] At each pressure, Brillouin spectra were collected in two scattering geometries – equal-angle transmission and backscatter. The measurements were performed on several cycles of compression and decompression, to a maximum pressure of 60 GPa. Each measured spectrum was folded about the central Rayleigh peak and fitted with Gaussian peaks to extract acoustic velocities [Gleason *et al.*, 2009]. We assigned the higher- and lower-frequency peaks to the compressional and shear modes, respectively.

[9] The sintered MgO sample gives shear- and compressional-wave velocities matching the single-crystal average at ambient conditions; when quasi-hydrostatically compressed, it gives velocities that also match single-crystal averages, and values for polycrystalline MgO loaded in NaCl [Murakami *et al.*, 2009] (Figure 1).

[10] In contrast, all of our non-hydrostatically loaded samples exhibit velocities significantly lower than the corresponding hydrostatic values at the same pressure (Figure 1). From 0–10 GPa, we observe shear and compressional wave speeds 2–3 km/s below the aggregate values for MgO (a drop of 30–50%) at ambient conditions. At roughly 10 GPa, there is a change in the observed pressure variation for  $V_p$  and  $V_s$  (both on compression and decompression of the pressed powder), with the velocity trend roughly parallel to that for the hydrostatically compressed aggregate between 10 and 60 GPa. For example, after compressing to 60 GPa and then decompressing to 35 GPa, we see a mode at 12.5 GHz, equivalent to 5.8 ( $\pm 0.1$ ) km/s, which we interpret to be the MgO shear mode at  $\sim 15\%$  lower velocity than the hydrostatic value of 6.8 km/s [Sinogeikin and Bass, 2000; Murakami *et al.*, 2009]. We observe the same anomalously low velocities for non-hydrostatically loaded MgO in the measurements performed in backscatter geometry (not shown) and in equal-angle scattering geometry (Figure 1); the analysis of the former requires knowledge of the sample's index of refraction, whereas the latter do not [Shimizu *et al.*, 1998]. Some of the Brillouin spectra exhibited only one of the two modes, either due to weak elasto-optic coupling (due to the combination of incident and scattered light polarizations), or overlapping of the MgO compressional mode and the diamond shear-mode at pressures above  $\sim 30$  GPa. We also note

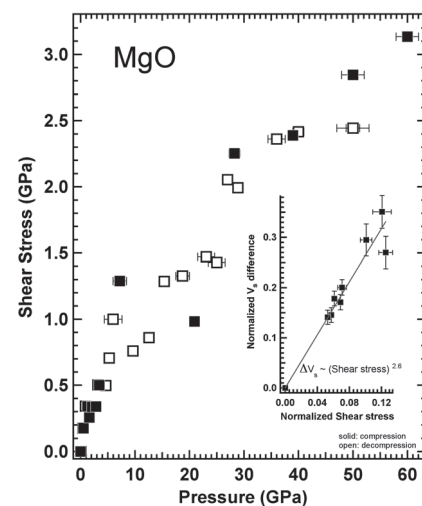


**Figure 2.** Maximum shear stress ( $\sigma_{shearstress}$ ) in polycrystalline MgO calculated as  $\sigma_{shearstress} = \frac{h}{2} \frac{dP}{dr}$ , where  $h$  is the sample thickness, and  $dP/dr$  is the measured pressure gradient based on spatial distribution of ruby spheres. *Inset:* velocity difference of the shear mode  $V_s$  (hydrostatic velocity - non-hydrostatic velocity) normalized by the hydrostatic velocity at the corresponding shear stress normalized by the measured pressure, only a few points shown for clarity.

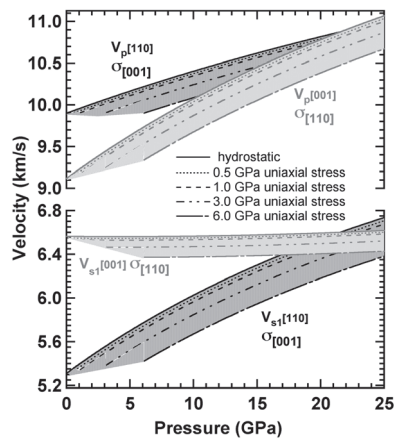


**Figure 3.** Calculated compressional ( $p$ ) and shear ( $s$ ) velocity trends for single-crystal MgO along the [001] and [110] crystallographic directions. Using density [Speziale *et al.*, 2001] and experimental third order elastic constants [Bogardus, 1965] the compressional and shear velocities in [001] and [110] directions [Bateman *et al.*, 1961; Mason, 1958] are calculated. These pressure dependent velocity trends under hydrostatic conditions (solid curves) are compared to the non-hydrostatic case, e.g., different values of applied uniaxial stress ( $\sigma$ ) (all dashed curves).

that peak profiles for polycrystalline data are generally broader than those of single crystals at the same pressure, reflecting the averaging over crystal orientations [Gleason *et al.*, 2009; Chen *et al.*, 2010].

[11] At each pressure, Brillouin spectra were collected at 4–8 locations evenly distributed around the sample chamber. Near these same locations within the sample chamber, the pressure was determined by way of ruby fluorescence, providing an estimate of pressure gradients across the sample. The sample thickness prior to compression is estimated to be 50  $\mu\text{m}$ , that is the measured thickness of the pre-indentation in the gasket. After decompression from 60 GPa, the gasket is removed from the diamond-cell and the new thickness is measured to be  $10 \pm 2 \mu\text{m}$  on average. The pressure gradient combined with a measure of the sample thickness before and after decompression allows for a calculation of the shear stresses [Meade and Jeanloz, 1988], (Figure 2). We correlate these shear stresses, normalized by the measured pressure, with the measured velocity offsets (as seen in Figure 1) between the hydrostatic single-crystal aggregate average and the non-hydrostatic trends normalized by the hydrostatic velocity. As the normalized shear stress increases over the pressure range of our experiments, 0–60 GPa, the normalized velocity difference also increases (Figure 2, inset).

[12] Prompted by our observation that non-hydrostatically loaded polycrystalline MgO velocities are substantially lower than the values under hydrostatic loading, we calculate the elastic effects of non-hydrostatic stresses on the sound velocities. Specifically, we use second- and third-order elastic constants to determine shear and compressional velocities in uniaxially compressed cubic crystals (Figure 3). Uniaxial compression serves here as a proxy for non-hydrostatic stress applied to a cubic single crystal.

[13] Following Bateman *et al.* [1961], we calculate the velocities under imposed uniaxial stresses of 0.5, 1.0, 3.0 or 6.0 GPa, plotting the difference between the velocity under hydrostatic and non-hydrostatic conditions in Figure 3: we find a 7% drop, at most. The calculations do indicate a velocity decrease in the plane perpendicular to the applied uniaxial stress for MgO, corresponding to the plane that is probed by our Brillouin scattering experiments. However, the magnitude of this effect – on its own – cannot account for our observations. Based on these calculations, it does not seem possible that the tens of percent velocity deviations we reproducibly measure for non-hydrostatically compressed MgO powder can be explained by the elastic effects of uniaxial stresses.

[14] Influences of texturing (preferred orientation) in monomineralic, polycrystalline MgO cannot account for our observed low velocities. The magnitude of those effects is at most  $\pm 6\%$  about the aggregate average velocity at all pressures studied here, as documented by the observed orientation-dependent velocity variations (elastic anisotropy) at high (quasi-hydrostatic) pressures, as well as the velocities calculated from second- and third-order elastic constants (Figure 1) [Schreiber *et al.*, 1973; Sinogeikin and Bass, 2000]. It is possible that combined effects of non-hydrostaticity and a strong degree of crystal preferred orientation (or texturing) could yield, at most, a 13% drop in velocities, however, we find that unlikely since this can only be reached at certain pressures and we document our non-hydrostatically loaded MgO exhibits only partial degrees of preferred orientation, using x-ray powder diffraction on our high-pressure samples. Note that MgO becomes acoustically isotropic at  $\sim 20$  GPa.

[15] MgO reacts with atmospheric moisture and hydrates to form  $\text{Mg}(\text{OH})_2$  (brucite); the anomalously low velocities we observe are comparable to those of brucite between 0 and 10 GPa [Jiang *et al.*, 2006]. However, we found no evidence of  $\text{Mg}(\text{OH})_2$  contamination in any of our samples based on either x-ray diffraction or Raman spectroscopy (see Figure S1 of the auxiliary material).<sup>1</sup>

[16] Using ultrasonic techniques, Yeheskel *et al.* [2005] found Young's modulus and the average shear modulus of nanocrystalline MgO to be lower by 13% than that of sub-micron grain-size MgO at zero pressure and room temperature. They propose that the decrease in elastic moduli is directly related to an increase in the volume fraction of grain boundaries. If our sample is crushed in the non-hydrostatic loading, the volumetric fraction of grain boundaries could increase, resulting in a Brillouin signal dominated by scattering from grain-boundary material, thereby showing decreased sound velocities. Thus, the influence of grain boundaries and crystallite size on Brillouin spectra – and on elastic properties more generally – need to be clarified in future studies (H. Marquardt *et al.*, Elastic properties of nano-crystalline MgO powder to high pressures by Brillouin light scattering, submitted to Physical Review B, 2011). A deeper understanding of these phenomena is essential for reliably characterizing non-hydrostatic effects on elastic properties of Earth materials.

<sup>1</sup>Auxiliary materials are available in the HTML. doi:10.1029/2010GL045860.

[17] **Acknowledgments.** A. Gleason was supported by the Carnegie/DOE Alliance Center for High Pressure Science and Technology, and H. Marquardt was supported by the German Academic Exchange Service (DAAD). Partial support also came from the US National Science Foundation and Department of Energy. We thank S. Clark, J. Yan, S. Raju and J. Knight (Lawrence-Berkeley National Laboratory) for technical collaboration, and are grateful for helpful discussions with B. Buffett, D. Dreger, G. Johnson, M. Manga and H.-R. Wenk (University of California, Berkeley), and R. O'Connell (Harvard University).

## References

- Armstrong, M. R., et al. (2008), Ultrafast high strain rate acoustic wave measurements at high static pressure in a diamond anvil cell, *Appl. Phys. Lett.*, *92*, 101930, doi:10.1063/1.2898222.
- Bateman, T., et al. (1961), Third-order elastic moduli of germanium, *J. Appl. Phys.*, *32*, 928–936, doi:10.1063/1.1736135.
- Birch, F. (1978), Finite strain isotherm and velocities for single-crystal and polycrystalline NaCl at high pressure and 300°K, *J. Geophys. Res.*, *83*(B3), 1257–1268, doi:10.1029/JB083iB03p01257.
- Bogardus, E. (1965), Third-order elastic constants of Ge, MgO, and fused SiO<sub>2</sub>, *J. Appl. Phys.*, *36*, 2504–2513, doi:10.1063/1.1714520.
- Buffett, B. (2006), Plate force due to bending at subduction zones, *J. Geophys. Res.*, *111*, B09405, doi:10.1029/2006JB004295.
- Campbell, A. J., and D. L. Heinz (1992), A high-pressure test of Birch's law, *Science*, *257*, 66–68, doi:10.1126/science.257.5066.66.
- Chen, B., et al. (2010), Elasticity, strength, and refractive index of argon at high pressure, *Phys. Rev. B*, *81*, 144110, doi:10.1103/PhysRevB.81.144110.
- Chen, D., et al. (2008), Pressureless sintering of translucent MgO ceramics, *Scr. Mater.*, *59*, 757–759, doi:10.1016/j.scriptamat.2008.06.007.
- Chung, W.-Y., and H. Kanamori (1980), Variation of seismic source parameters and stress drops within a descending slab and its implications in plate mechanics, *Phys. Earth Planet. Inter.*, *23*, 134–159, doi:10.1016/0031-9201(80)90008-4.
- Conrad, C. P., and B. Hager (1999), Effects of plate bending and fault strength at subduction zones on plate dynamics, *J. Geophys. Res.*, *104*(B8), 17,551–17,571, doi:10.1029/1999JB900149.
- Fukao, Y., and M. Kikuchi (1987), Source retrieval for mantle earthquakes by iterative deconvolution of long-period P-waves, *Tectonophysics*, *144*, 249–269, doi:10.1016/0040-1951(87)90021-7.
- Gleason, A. E., B. Chen, and R. Jeanloz (2009), Grain-boundary effects in Brillouin scattering at ambient and high pressure, *Geophys. Res. Lett.*, *36*, L23309, doi:10.1029/2009GL040420.
- Ishii, M., and J. Tromp (1999), Normal-mode and free-air gravity constraints on lateral velocity variations in velocity and density of Earth's mantle, *Science*, *285*, 1231–1236, doi:10.1126/science.285.5431.1231.
- Jackson, I., and H. Niesler (1982), The elasticity of periclase to 3 GPa and some geophysical implications, in *High Pressure Research in Geophysics*, edited by S. Akimoto and M. H. Manghnani, pp. 93–113, Cent. Acad. Publ. Jpn., Tokyo.
- Jiang, F., et al. (2006), Single-crystal elasticity of brucite, Mg(OH)<sub>2</sub>, to 15 GPa by Brillouin scattering, *Am. Mineral.*, *91*, 1893–1900, doi:10.2138/am.2006.2215.
- Kanamori, H. (1980), State of stress in the Earth's lithosphere, in *Physics of the Earth's Interior, Proc. Int. Sch. Phys. "Enrico Fermi"*, edited by A. M. Dziewonski and E. Boschi, pp. 531–552, North-Holland, Amsterdam.
- Kanamori, H., et al. (1998), Frictional melting during the rupture of the 1994 Bolivian earthquake, *Science*, *279*, 839–842, doi:10.1126/science.279.5352.839.
- Kaus, B., et al. (2009), Lithospheric stress-state predicted from long-term tectonic models: Influence of rheology and possible application to Taiwan, *J. Asian Earth Sci.*, *36*, 119–134, doi:10.1016/j.jseas.2009.04.004.
- Mao, H. K., et al. (1978), Specific volume measurements of Cu, Mo, Pd, and Ag and calibration of the ruby R1 fluorescence pressure gauge from 0.06 to 1 Mbar, *J. Appl. Phys.*, *49*, 3276–3283, doi:10.1063/1.325277.
- Marquardt, H., et al. (2009), Elastic shear anisotropy of ferropericlase in Earth's lower mantle, *Science*, *324*, 224–226, doi:10.1126/science.1169365.
- Mason, W. (1958), *Physical Acoustics and the Properties of Solids*, pp. 368–380, D. Van Nostrand, Princeton, N. J.
- Meade, C., and R. Jeanloz (1988), Yield strength of MgO to 40 GPa, *J. Geophys. Res.*, *93*(B4), 3261–3269, doi:10.1029/JB093iB04p03261.
- Munguia, L., and J. Brune (1984), High stress drop events in the Victoria, Baja California earthquake swarm of 1978 March, *Geophys. J. R. Astron. Soc.*, *76*, 725–752.
- Murakami, M., et al. (2009), Elasticity of MgO to 130 GPa: Implications for lower mantle mineralogy, *Earth Planet. Sci. Lett.*, *277*, 123–129, doi:10.1016/j.epsl.2008.10.010.
- Reichmann, H., et al. (2008), Single-crystal elastic properties of (Mg<sub>0.987</sub>, Fe<sub>0.013</sub>)O to 9 GPa, *Am. Mineral.*, *93*, 1306–1311, doi:10.2138/am.2008.2717.
- Ruff, L. J. (1999), Dynamic stress drop of recent earthquakes: Variations within subduction zones, *Pure Appl. Geophys.*, *154*, 409–431, doi:10.1007/s000240050237.
- Schreiber, E., et al. (1973), *Elastic Constants and Their Measurements*, pp. 25–31, McGraw-Hill, New York.
- Shimizu, H., et al. (1998), High-pressure elastic properties of liquid and solid krypton to 8 GPa, *Phys. Rev. B*, *57*, 230–233, doi:10.1103/PhysRevB.57.230.
- Simmons, G., and H. Wang (1971), *Single Crystal Elastic Constants and Calculated Aggregate Properties: A Handbook*, 2nd ed., pp. 10–11, MIT Press, Cambridge, Mass.
- Sinogeikin, S., and J. Bass (2000), Single-crystal elasticity of pyrope and MgO to 20 GPa by Brillouin scattering in the diamond cell, *Phys. Earth Planet. Inter.*, *120*, 43–62, doi:10.1016/S0031-9201(00)00143-6.
- Spetzler, H. (1970), Equation of state of polycrystalline and single-crystal MgO to 8 kilobars and 800°K, *J. Geophys. Res.*, *75*(11), 2073–2087, doi:10.1029/JB075i011p02073.
- Speziale, S., et al. (2001), Quasi-hydrostatic compression of magnesium oxide to 52 GPa: Implications for the pressure-volume-temperature equation of state, *J. Geophys. Res.*, *106*(B1), 515–528, doi:10.1029/2000JB900318.
- Watts, A. B. (1978), An analysis of isostasy in the world's oceans: 1. Hawaiian-Emperor Seamount Chain, *J. Geophys. Res.*, *83*(B12), 5989–6004, doi:10.1029/JB083iB12p05989.
- Yehekel, O., et al. (2005), Elastic moduli of grain boundaries in nanocrystalline MgO ceramics, *J. Mater. Res.*, *20*(3), 719–725, doi:10.1557/JMR.2005.0094.

B. Chen, A. E. Gleason, and R. Jeanloz, Department of Earth and Planetary Science, University of California, Berkeley, 307 McCone Hall, CA 94720-4767, USA. (aegleson@lbl.gov)

H. Marquardt, S. Speziale, GFZ German Research Centre for Geosciences, Telegrafenberg, D-14473 Potsdam, Germany.

J. Wu, Material Sciences Division, Lawrence Berkeley National Laboratory, 1 Cyclotron Rd., MS 62R0203, Berkeley, CA 94720, USA.